



Time-averaged paleomagnetic field and secular variation: Predictions from dynamo solutions based on lower mantle seismic tomography

Christopher J. Davies^{a,*}, David Gubbins^a, Ashley P. Willis^b, Peter K. Jimack^c

^a School of Earth and Environment, University of Leeds, Leeds LS2 9JT, UK

^b Department of Mathematics, University of Bristol, University Walk, Bristol BS8 1TW, UK

^c School of Computing, University of Leeds, Leeds LS2 9JT, UK

ARTICLE INFO

Article history:

Received 18 February 2008

Received in revised form 4 July 2008

Accepted 5 July 2008

Keywords:

Geomagnetism

Paleomagnetic time average

Paleomagnetic secular variation

Dynamo

ABSTRACT

We compare three dynamo solutions incorporating laterally varying boundary heat flux with paleomagnetic models and data. The boundary condition is defined by the D'' seismic shear-wave velocity and the three solutions have boundary anomalies with different amplitudes. The generated fields appear to divide into a stationary, boundary-locked part and a time-varying part with persistent centres of activity. Both parts contribute to the time average. A very long averaging time can be needed for nearly-locked solutions, but a rough time average that remains within the threshold set by the accuracy of paleomagnetic data is achieved in a few diffusion times. The locked part dominates for larger amplitude boundary anomalies. In previous work the locked field was shown to have strong similarities with the modern geomagnetic field. Previous dynamo solutions that were not locked to the boundary show similarities with our solutions with weak boundary forcing. The axisymmetric time average has small g_2^0 and larger g_3^0 components and peaks in inclination anomaly in high latitudes (associated with the locked field) and low latitudes (associated with the time average of the time-varying fields). The non-axisymmetric time average displays a striking longitudinal variation in inclination anomaly, with a large negative anomaly in the Pacific region in agreement with observations. None of the dominant geomagnetic coefficients are axisymmetric and g_2^0 negligible in all three models. Secular variation is concentrated in equatorial latitudes, as in some recent paleomagnetic models. The locked field agrees with the inclination difference found between Hawai'i and Réunion, in agreement with paleomagnetic averages. The locked field agrees with the paleomagnetic time average rather better than the fields with less boundary variations. We conclude that, because the locked field agrees with the modern field as well as some aspects of the long-term time average, the geomagnetic field spends a considerable time in the present four-lobe configuration: it is not a coincidence that the present field resembles the time average. Longitudinal variations are likely to be at least as important as latitudinal variations in the paleomagnetic time average. This presents a challenge for dynamo theory, since a move to more geophysically realistic parameters would appear to destroy the locked solutions.

© 2008 Elsevier B.V. All rights reserved.

1. Introduction

Lower mantle convection takes place on timescales much longer than those associated with core convection and is subjected to a uniform lower boundary temperature. The outer core is therefore subjected to an imposed laterally varying heat flux on its upper boundary. It is then inevitable that the outer core is influenced by the overlying mantle; the only question is whether the mantle's influence is detectable in observations. In this paper we compare dynamo simulations incorporating laterally varying heat

flux boundary conditions with paleomagnetic data to ascertain whether observational data contain a signature of thermal mantle control.

There is now a body of observational evidence pointing towards core–mantle coupling: four ‘lobes’ of intense magnetic flux, symmetrically displaced about the equator at high latitudes, are observed in historical (Bloxham and Gubbins, 1985; Jackson et al., 2000) and paleomagnetic (Kelly and Gubbins, 1997; Korte and Constable, 2005) models; sediment (Laj et al., 1991) and lava (Love, 1998) data indicate that paths traversed by virtual geomagnetic poles (VGPs) during geomagnetic reversals appear to prefer one of two longitudes; and secular variation in the Pacific hemisphere appears persistently low (Doell and Cox, 1972; Johnson and Constable, 1998). These observations indicate departures from

* Corresponding author.

E-mail address: c.davies@see.leeds.ac.uk (C.J. Davies).

spherical symmetry, which can only be caused by boundary inhomogeneities.

A heat flux map of the core–mantle boundary (CMB) may be derived by using seismic shear-wave velocity as a proxy for heat flux. This assumes that variations in seismic shear-wave velocity are due to temperature (rather than compositional) variations in the lower mantle boundary layer, and because the CMB is isothermal, such temperature differences generate lateral variations in heat flux conducted through the lower mantle boundary layer. We use the seismic shear-wave model of Masters et al. (1996); it comprises a spherical harmonic map of heat flux at the CMB out to degree 12 and contains a large term of harmonic degree and order 2. We are therefore testing two hypotheses: (1) that D'' seismic anomalies are correlated with temperature and (2) that CMB heat flux variations create a detectable paleomagnetic signal.

Many previous studies have incorporated inhomogeneous core–mantle coupling derived from seismic tomography (e.g. Glatzmaier et al., 1999; Kutzner and Christensen, 2004; Aubert et al., 2007; Christensen and Olson, 2003). Using a 2.5D model, Sarson et al. (1997) found nearly steady dynamos with flux lobes lying over regions of high heat flux, consistent with studies of locking of thermal convection to boundary heterogeneities (Zhang and Gubbins, 1993). The dynamically self-consistent models of Bloxham (2002) supported this. Bloxham (2000), also using the tomographic model of Masters et al. (1996), was able to match numerical and observed magnitudes of secular variation (SV). He found a rapid increase in SV near the equator but no average difference in SV between the Pacific and Atlantic hemispheres. Olson and Christensen (2002) used a variety of inhomogeneous boundary conditions to investigate time-averaged properties of simulated magnetic fields. Their results for the tomographic boundary condition are closest to the results reported here and we discuss these at length in Section 4.

The above examples generally produced magnetic fields that varied too rapidly in time to allow direct correlation with the observed geomagnetic field. Gubbins et al. (2007) (see also Willis et al., 2007) were the first to produce dynamos with fields that lock to the CMB thermal anomalies for many magnetic diffusion times. The striking similarities between their solutions and the historical field encouraged us to make comparisons with paleomagnetic data. We make comparisons with the time-averaged paleomagnetic field, paleosecular variation (PSV), and paleomagnetic data from Hawai'i and Réunion Island.

This paper is organised as follows. In Section 2 we discuss the dynamo solutions of Gubbins et al. (2007), time averaging, and limitations imposed by the choices of input parameters. Results for the time-averaged field and PSV data are reported in Section 3 along with a comparison to data from Hawai'i and Réunion Island. Discussion and conclusions are presented in Section 4.

2. Method

We use the magnetic fields generated by the three dynamo models reported in Gubbins et al. (2007) and in further detail by Willis et al. (2007). These solutions were found by timestepping the equations of momentum, heat, and magnetic induction using a pseudospectral code. The fluid is contained in a rotating spherical shell with aspect ratio 0.35. The temperature is fixed on the lower boundary; on the outer boundary the heat flux is prescribed to be proportional to the seismic shear-wave velocity of the lowermost mantle in the tomographic model of Masters et al. (1996). Rigid velocity boundary conditions are used and the inner core is conducting but not free to rotate.

The governing non-dimensional equations depend on α the thermal expansion coefficient, g the acceleration due to gravity, Ω

the spin rate, β the mean temperature gradient imposed at the core surface, κ the thermal diffusivity, ν the kinematic viscosity, η the magnetic diffusivity, and d the shell width. These are combined into five non-dimensional parameters whose numerical values were chosen to favour *locked* solutions with strong correlations between the generated field and boundary anomalies:

- *Ekman number*, the ratio of viscous and Coriolis forces, $E = \nu/2\Omega d^2 = 1.2 \times 10^{-4}$, was set low enough for the dynamics to be dominated by rotation (as in the real Earth) but large enough to allow computations to be completed in a reasonable amount of time.
- *Prandtl number*, the ratio of kinematic viscosity and thermal diffusion, $Pr = \nu/\kappa = 1$, is kept large enough to retain the desired magnetostrophic balance in which inertia plays a secondary role.
- *Rayleigh number*, measuring the strength of the buoyancy force, $Ra = g\alpha\beta d^5/\kappa\nu = 1.5R_c$, where R_c is the critical Rayleigh number for the onset of non-magnetic convection with homogeneous boundary conditions. Ra is kept low so as to obtain solutions that were as steady as possible.
- *Roberts number*, the ratio of thermal and magnetic diffusion, $q = \kappa/\eta = 10$, must be kept large (given choices already made for the other parameters) for dynamo action to occur.
- *Horizontal Rayleigh number*, Ra_H , measuring the strength of lateral variations in heat flux through the lower mantle boundary layer. The parameter $\epsilon = Ra_H/Ra$ measures the peak-to-peak variation of heat flux on the boundary relative to the average heat flux leaving the core.

Sets of synthetic geomagnetic coefficients $\{g_l^m, h_l^m\}$ are computed at each time point for comparison with data. This paper is restricted to exploring the effects of changing ϵ , the amplitude of lateral surface heating, for fixed vertical heating.

Here we use three solutions for $\epsilon = 0.3, 0.6$ and 0.9 in order to assess the influence of boundary variations. These solutions have time averages showing one remarkable property: their generated magnetic fields on the outer surface tend to concentrate in four main lobes in similar locations to those of the historical geomagnetic field. When boundary variations are strong ($\epsilon = 0.9$) the field is almost stationary and the lobes lie within about 5° of the corresponding locations on the surface of the Earth's core. No dynamo action occurs for $\epsilon = 0$ or ϵ much above 1, so we cannot compare our results with those for homogeneous boundary conditions and we cannot lock the solutions more tightly to the boundary. A similar problem was encountered by Olson and Christensen (2002) in a related study.

The surface field for the $\epsilon = 0.9$ solution is nearly stationary with four dominant high latitude concentrations of flux. The time dependence is dominated by small movements of these lobes and the occasional appearance of “clover-leaf” patterns of flux near two equatorial centres at longitudes $\phi = \pm 90^\circ$ that sometimes detach and drift west. In the $\epsilon = 0.6$ solution the main lobes are intermittent and more mobile, particularly the western pair, and the equatorial patches drift more readily. In the $\epsilon = 0.3$ solution the main lobes are less stable still and the equatorial region more active.

The whole group of solutions are characterised by a locked part, revealed most clearly in the $\epsilon = 0.9$ solution, and a time-varying part with persistent centres of activity, most notably beneath Indonesia and Central America, with westward drift of flux patches between these centres. The behaviour of the main lobes at high latitudes appears to be independent of the behaviour at low latitudes. The persistent nature of the low latitude centres of activity means that they contribute to a time average, and we might therefore be able to separate it from the locked part by comparing time averages at different values of ϵ .

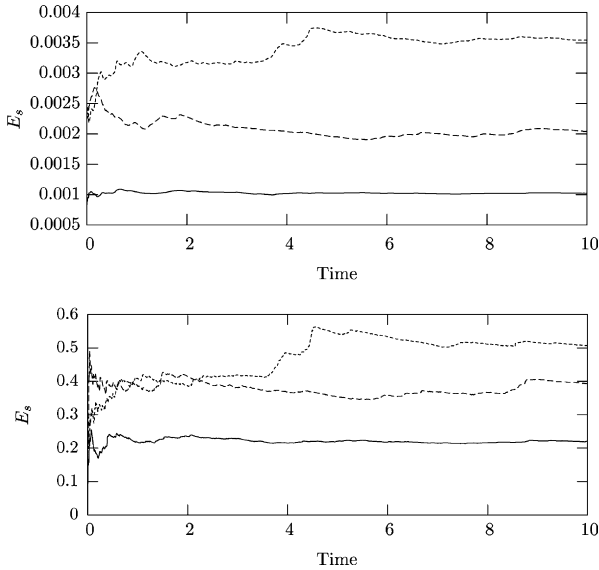


Fig. 1. E_s and its time derivative, \dot{E}_s , as a function of time for $\epsilon = 0.3$ (short-dashed line), $\epsilon = 0.6$ (dashed line) and $\epsilon = 0.9$ (solid line). Time is measured in units of the magnetic diffusion time (100 kyr). Periods of “hang up” are clearest for $\epsilon = 0.3$ from $t = 1$ –4 and $t = 5$ –10 while change in field configuration is evident between $t = 4$ and 5. The $\epsilon = 0.9$ solution reaches a steady state within two magnetic diffusion times.

Some of the parameters are far from the values thought to be correct for the Earth, but the same is true for all numerical geodynamo models (except perhaps for the large Roberts number, a limitation that might be removed in future work by changing the buoyancy profile; Sreenivasan and Gubbins, 2008). This means we must be cautious in what we compare with observation.

First, we have done nothing to force the overall magnetic field strength to match that of the Earth; we should not therefore expect the absolute intensity to be right. We could adjust Ra to improve this, but it would take us out of the locked regime and perhaps even out of the magnetostrophic regime thought to hold in the Earth’s core. The field intensity decreases as ϵ increases because the stronger lateral variations in surface heat flux tend to concentrate downwelling and focus magnetic flux into smaller features, which attenuate strongly when upward continued to the Earth’s surface. This is not an effect we could hope to detect with paleomagnetic data. Secondly, E is too large, which is likely to affect the short-term SV in particular.

This leaves the geographical morphology of the time-averaged field and long-term SV. The spectacular correspondence of the four main lobes of the locked fields and those of the historical geomagnetic field reported in Gubbins et al. (2007) encourage us to make comparisons with paleomagnetic data. We also make comparison with PSV data; again we do not expect to have successfully modelled the amplitude of the PSV because the solutions are tightly locked to the boundary, we are interested only in geographical variations.

We obtain time averages from the models by simple time integration. Inspection of the plots of averaged inclination, intensity, and their standard deviations suggests the sufficient averaging time decreases with ϵ : $\tau_{ave} = 5.0, 4.0, 1.5$ for $\epsilon = 0.3, 0.6, 0.9$. We attempted to verify this by plotting the time-integral of the surface energy:

$$E_s = \int B^2 dS = \sum_{l,m} (l+1) [(g_l^m)^2 + (h_l^m)^2] \quad (1)$$

and its time derivative as functions of time (Fig. 1). Separate averaging times are required for secular variation because there is no reason to suppose they are the same as for main field.

A decrease in averaging time with ϵ seems reasonable because models with a higher ϵ are more tightly locked to the boundary and therefore have less time dependence, but this argument is naïve. Consider the simple case of locked non-magnetic convection with temperature boundary conditions studied by Zhang and Gubbins (1993). For homogeneous boundary conditions the convection takes the form of a few rolls drifting steadily in azimuth; the flow is periodic in time and stationary in a co-rotating frame of reference. The flow continues to be periodic in time after lateral variations of temperature are imposed on the boundary but the drift rate becomes uneven, slowing down when a rising limb of a convection roll falls beneath a hot part of the boundary and speeding up when it falls beneath a cold part of the boundary. As boundary variations (ϵ) are increased further, the flow becomes stationary, locked into a position with rising limbs beneath hot boundary, the most favourable configuration for convection. The bifurcation between the stable locked solution and the unevenly drifting solution is a saddle node and the instability sets in as a wave of infinite period.

The averaging time required for this flow is exactly one period of the periodic solutions. At $\epsilon = 0$ this is the time for one roll to pass a point on the boundary; for $\epsilon > 0$ uneven drifting may increase or decrease the period but eventually it must increase it because the flow spends more time close to the stable, locked, position. Finally, as the saddle point is approached, the averaging time goes to infinity: then, as the critical value of ϵ is passed and the flow becomes steady, the averaging time falls abruptly to zero! This shows that even simple regimes exist where larger boundary anomalies cause larger averaging times.

Unfortunately no dynamos are known that exhibit such simple behaviour, but even in our more complex, “locked”, dynamos it is possible for the flow to “hang up” on a boundary anomaly for a time. The solutions for $\epsilon = 0.3$ and 0.6 both have quite long intervals when four main lobes appear, followed by intervals when the field is rather chaotic. The field can be in quite different configurations each time it “hangs up”. Behaviour like this is responsible for the rise between $t = 4$ and 5 seen for $\epsilon = 0.3$ in Fig. 1. We cannot therefore assume a short averaging time for these dynamos, and even 10 diffusion times may not be long enough to produce a good time average. For the practical purposes of this paper, comparison with paleomagnetic data, an average over the entire run of about 10 diffusion times is satisfactory because the plots and numerical values we use are changing by less than the errors in the data.

A further problem arises when interpreting any dimensionless time in terms of real times because of the compromised choice of parameters. The relevant intrinsic physical timescales are those of magnetic diffusion and advection. We choose $\eta = 1.6 \text{ m}^2 \text{ s}^{-1}$ as typical for the core, which gives a diffusion time $\tau_\eta = d^2/\eta = 100 \text{ kyr}$, the same for all models. The more usual measure of the diffusion time is that for a dipole field to fall by a factor e : here $\tau_{dip} = c^2/\pi^2\eta = 25 \text{ kyr}$, where c is the core radius. The advection time is $\tau_v = d/v$, where v is the mean velocity calculated from the kinetic energy, $v = \sqrt{2K.E.}$ This gives $\tau_v = 200 \text{ yr}$. The corresponding magnetic Reynolds number is $R_m = 500$. The flow is dominated by the toroidal component, the poloidal part comprising only 20% of the total kinetic energy. The rise time is therefore approximately $\sqrt{5}\tau_v$ and the overturn time, the time taken for a fluid particle to traverse the core and return to its original position, the usual measure of advection, is twice the rise time, or about 1000 yr. These are all reasonable geophysical numbers. The only unfortunate consequence of fixing η first is that the combination of $q = 10, Pr = 1, E = 1.2 \times 10^{-4}$ requires $2\pi/\Omega = 15 \text{ yr}$: the day in this model is 15 yr

long. This problem is common to all numerical geodynamo solutions to some extent.

This dimensionalisation gives averaging times for our three models of 150, 400 and 500 kyr, much longer than the advection time, but even these long times do not produce a completely stationary solution: integration of well over 1 Myr might be needed for this. All time averages used in this paper are for more than 10 magnetic diffusion times. Carlot et al. (1999) found that at least 10 kyr is needed to extract the mean field if the recent field is representative of the past. Merrill and McFadden (2003) reviewed the subject and endorse the (seemingly unwritten) idea that 5 Myr is an adequate period to obtain the true average field. We do not believe too much should be read into the averaging times for the three dynamo models used in this paper; a more thorough study of the effect on determining paleomagnetic poles from a larger class of dynamo models is required.

Most analyses of paleomagnetic data have concentrated on the axisymmetric time average, and we deal with this first. We check for departures from the geocentric axial dipole (GAD), equatorial symmetry, and influence of the tangent cylinder. The morphology of the 3D time-averaged field is explored by plotting the inclination anomaly $\Delta I = I - I_D$, where I is the measured inclination and I_D the dipole inclination, relative total field anomaly $\Delta F = F - F_D$, where F_D is the dipole intensity and F is the intensity of the field normalised by g_1^0 , and declination D . We also examine relative sizes of geomagnetic coefficients out to degree 4. PSV is estimated by calculating the standard deviations of I , D , and F , and the VGP scatter function defined in the usual way as

$$S^2 = \frac{1}{N} \sum_{i=1}^N \Delta_i^2 \quad (2)$$

where Δ_i is the angular distance between the i th VGP and the mean VGP position. A dynamo model for the entire field gives us the luxury of comparing predictions at specific sites with observations at those sites, and we focus on Hawai'i and Réunion using the recent study of Love and Constable (2003).

3. Results

3.1. Axisymmetric field

Fig. 2 shows the axisymmetric inclination anomaly as a function of latitude θ for the three cases $\epsilon = 0.3, 0.6, 0.9$. All three curves show two pairs of maxima and minima, one at high latitude and one at low latitude. The high latitude extrema are most prominent in the locked solution with $\epsilon = 0.9$; the low latitude extrema are larger for the weakly locked $\epsilon = 0.3$ and 0.6 solutions.

It would seem that the high latitude extrema in Fig. 2 are associated with the main lobes of the locked field and those at low latitude are associated with the time-averaged secular variation around the equator. The main lobes dominate at $\epsilon = 0.9$, the locked solution, because they persist and the secular variation is relatively small. The SV events dominate the $\epsilon = 0.6$ and 0.3 solutions, which explains the larger low-latitude extrema in Fig. 2. Non-dipole intensities (Fig. 2) are very small except near the poles. This is the effect of weak flux within the tangent cylinder. The anomalies elsewhere are less than 10% and it would therefore be difficult to detect with paleointensity data, a single site measurement having an error of 10% or more. Table 1 gives the numerical values of the first three axisymmetric geomagnetic coefficients. Dimensional values of g_1^0 are geophysically reasonable but we attach little significance to this. Relative quadrupole terms G_2^0 are all significantly smaller than paleomagnetic estimates and are the opposite sign (cf. Merrill et al., 1996). Octupole components are comparable with, or larger than,

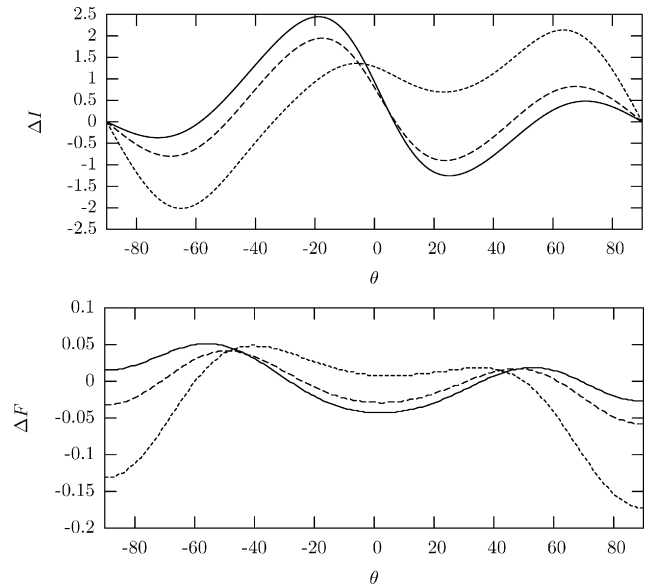


Fig. 2. Axisymmetric inclination anomaly (top) and normalised intensity anomaly for $\epsilon = 0.3$ (solid line), $\epsilon = 0.6$ (dashed line) and $\epsilon = 0.9$ (short-dashed line). ΔI shows two pairs of maxima and minima in both hemispheres for each value of ϵ . Departures of F from a dipole exceed 10% only in polar regions.

the corresponding quadrupole component. A similar result was found by Olson and Christensen (2002); the preference of these dynamo models for octupole fields may reflect a high degree of equatorial symmetry.

3.2. Nonaxisymmetric field

Fig. 3 shows the time-averaged intensity anomaly, inclination anomaly and declination for the three values of ϵ . There are considerable and surprising variations with ϵ . We attribute the differences to the separate time-varying and locked contributions in each solution. The solution for $\epsilon = 0.9$ is dominated by the locked field and its four main lobes, which give the highs in intensity and four blue–red pairs in declination. Solutions for $\epsilon = 0.3$ and 0.6 are strongly influenced by equatorial time-dependent activity on the CMB as well as smoothing of the four main lobes caused by drift and intermittency. This leaves just two blue–red pairs in the declination plot and a dominant low equatorial ring in intensity. The inclination maps are also smeared out in longitude.

We do not attempt any comparisons of the intensity anomalies with data because the anomalies are too weak and paleointensity measurements too inaccurate for any comparison to be meaningful. The inclination anomalies, on the other hand, are large compared with the error in a single paleomagnetic measurement. The peak anomalies are $\pm 8^\circ$, easily detectable by paleomagnetism. The plot for $\epsilon = 0.9$ in Fig. 3 shows a large negative anomaly in the Pacific

Table 1

Leading axisymmetric geomagnetic coefficients in units of nT and ratios of individual Gauss coefficients $G_2^0 = g_2^0/g_1^0$ and $G_3^0 = g_3^0/g_1^0$ for each of the three models

Coefficient	$\epsilon = 0.3$	$\epsilon = 0.6$	$\epsilon = 0.9$	Merrill et al. (1996)
g_1^0	−70,654	−53,436	−38,261	–
g_2^0	621	362	399	–
g_3^0	−992	−258	736	–
G_2^0	−0.0088	−0.0068	−0.0104	0.04
G_3^0	0.0141	0.0048	−0.0192	0.01

Merrill et al.'s (1996) time-averaged paleomagnetic Brunhes data is also included for comparison.

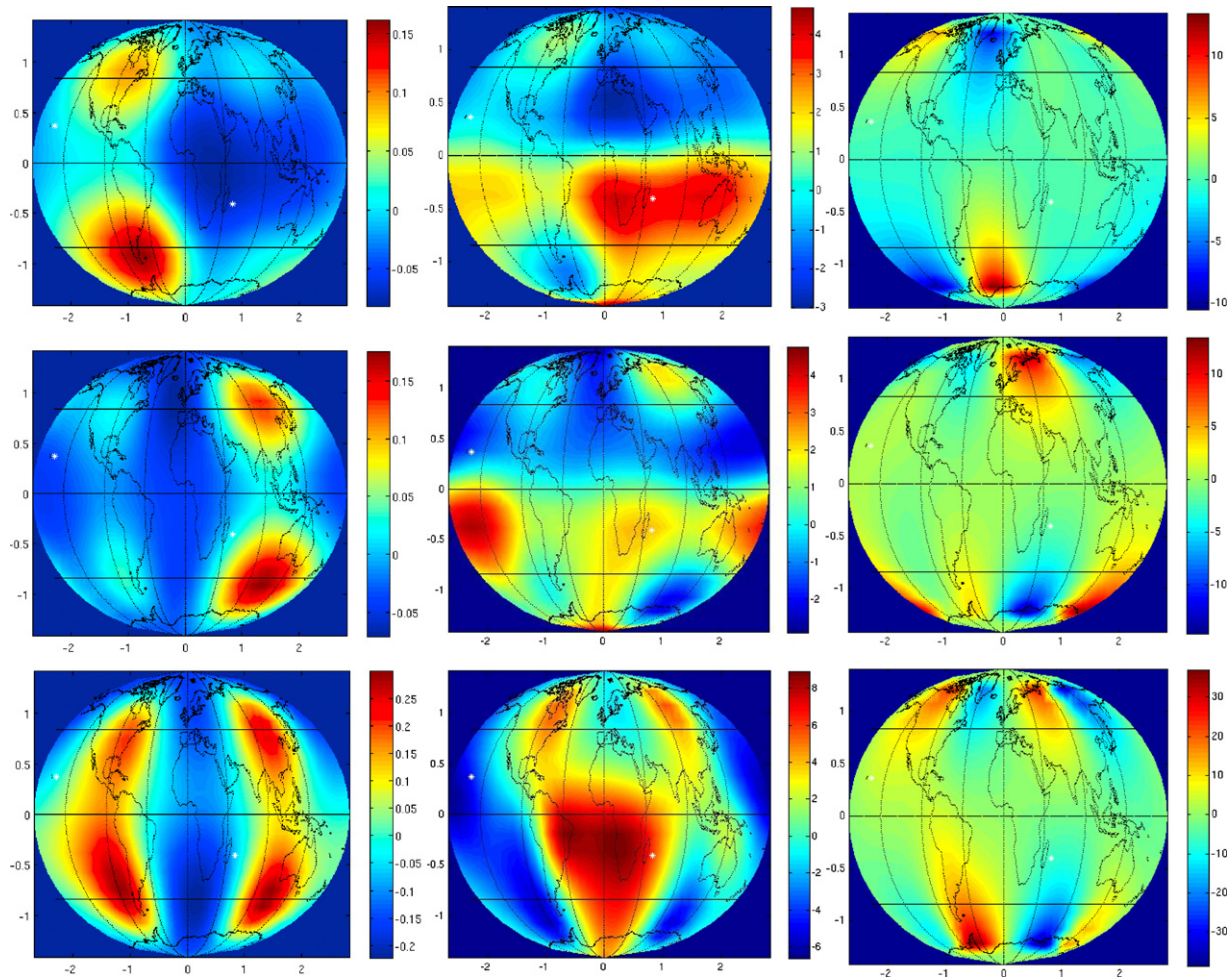


Fig. 3. Time-averaged intensity anomaly (left), inclination anomaly (middle) and declination (right) for each of the three cases $\epsilon = 0.3$ (top row), $\epsilon = 0.6$ (middle row) and $\epsilon = 0.9$ (bottom row). Note the differences with ϵ , showing that the low-latitude time-varying parts of the field contribute to the time average. Stars show the locations of Hawai'i and Réunion Island. (For interpretation of the references to colour in the citation of this figure legend, the reader is referred to the web version of the article.)

region and a large positive anomaly under southern Africa and the south Atlantic. This reflects the slight displacement of the four main lobes towards the Pacific hemisphere: they are not symmetrically placed in longitude but are separated by about 190° (Gubbins et al., 2007). The most striking thing about the plot is the enormous variation in longitude, which is greater than the variation in latitude.

These inclination anomalies do not appear in the historical field but several paleomagnetic studies support the idea of a negative inclination anomaly in the Pacific; it appears in the 3 kyr model of Constable et al. (2000) and the 7 kyr model of Korte and Constable (2005), although the dynamo prediction is weaker ($\sim 6^\circ$ compared to $\sim 10^\circ$ for Korte and Constable, 2005). Negative inclinations have also been reported in more recent studies (Elmaleh et al., 2001; Herrero-Bervera and Valet, 2003). Constable et al. (2000) find a positive anomaly in the south African region, displaced eastward to that of our dynamo model. The fits to observations of the $\epsilon = 0.3$ and 0.6 solutions are much less convincing.

Declination maps (Fig. 3) show lobe-like formations emanating from polar regions, which are visible in the archaeomagnetic and, to a lesser extent, historical models (Korte and Constable, 2005; Jackson et al., 2000). However, the overall morphology of the maps is very different, and the historical and archaeomagnetic maps differ significantly from each other, so it is difficult to draw significant conclusions from declination. The $\epsilon = 0.9$ solution has

four pairs of lobes in each hemisphere, reflecting the four lobes of the locked field, while $\epsilon = 0.3$ and 0.6 solutions have only two pairs.

It is also instructive to look at the low-order relative geomagnetic coefficients (Fig. 4). The non-dipole and non-axisymmetric terms increase with ϵ , as expected because the boundary condition places a longitudinal preference on the solution. The axisymmetric coefficients G_2^0 (where $G_l^m = g_l^m/g_0^0$ and similar for H_l^m) and G_3^0 are not the largest in any of the cases, the quadrupole term being insignificant in all three models.

An anonymous reviewer has queried the small values of G_2^0 in Fig. 4, indicating that the value of G_2^0 over the past 5 Myr is believed to be better constrained than the values of the non-axisymmetric coefficients, which are large in our models. Most of these studies have only considered axisymmetric coefficients in their time-averaged field models and hence have not constrained the non-axisymmetric harmonics. When non-axisymmetric fields are included they tend to be significant, as in the time-averaged field models of Kelly and Gubbins (1997) and Johnson and Constable (1995). This issue is discussed further in Gubbins (1998). G_2^0 also displays substantial variability in historical field models, changing sign in the model of Jackson et al. (2000) (see Jackson and Finlay, 2007).

The largest non-axisymmetric terms for the $\epsilon = 0.9$ model are G_1^1 , G_2^1 and G_3^2 , while H_2^1 is prominent for the lower values of ϵ . This

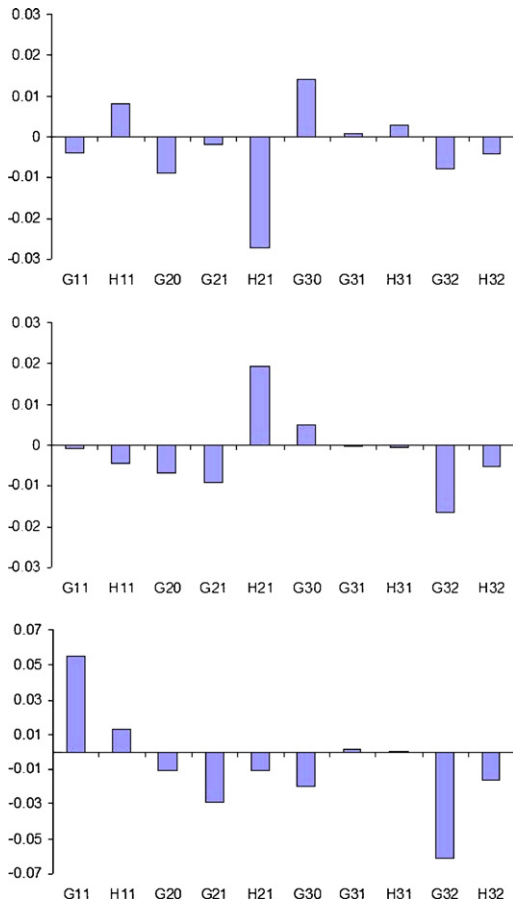


Fig. 4. Ratios of various low-degree harmonics as a percentage of the axial dipole value. The three cases are $\epsilon = 0.3$ (top), $\epsilon = 0.6$ (middle) and $\epsilon = 0.9$ (bottom). Contributions of axisymmetric coefficients are small in all cases while non-axisymmetric terms increase with ϵ .

harmonic features in PSV models (e.g. Gubbins and Kelly, 1995) and its appearance for the low ϵ models may be another indication of the influence of persistent SV on the time-averaged field.

3.3. Paleosecular variation

Fig. 5 shows the standard deviations of F , σ_F , and I , σ_I , measures of the time variations in the model. Plots of σ_D , the standard deviation of declination, are not informative as they are dominated by the increase towards the poles caused by the singularities there. The intensity plots are surprisingly similar to their time-averaged counterparts in Fig. 3, suggesting the main time variations are pulsations of the four main lobes with little movement. The inclination plots have large positive anomalies round the equator for all three models, showing that SV is dominated by the westward-drifting anomalies that are seen shedding from two equatorial centres on the CMB near the downwelling limbs. Increasing ϵ decreases the anomalies, particularly beneath the swath between Indonesia and the south Atlantic. These models do not show any evidence of low SV in the Pacific. There is a clear similarity in the form of σ_I between our models and that of Constable et al. (2000). The $\epsilon = 0.3$ solution displays three foci, which are also visible in the Constable et al. (2000) model, albeit with a phase difference. The large degree of variation in the Pacific for all models is also in agreement with Constable et al. (2000).

Fig. 6 shows the VGP scatter as a function of latitude for the three values of ϵ . The function is strongly symmetric about the

equator. Many paleomagnetic studies have assumed this despite a lack of southern hemisphere coverage (e.g. Merrill et al., 1996). Although the modern field is strongly asymmetric about the equator, this is a recent event associated with the reversal of flux in parts of the southern hemisphere; prior to AD1800 the historical model of Jackson et al. (2000) gives a symmetric VGP scatter function. For all the models S^2 increases towards the poles, as it does for the Earth. This is surprising because the maps of standard deviation show strongest SV in low latitudes (Fig. 5); the rise with latitude would seem to be a result of the VGP transformation rather than a real measure of increased SV. The VGP scatter in the models is substantially smaller than that obtained from paleomagnetic data (e.g. McFadden et al., 1988, 1991). This is probably because the models are tightly locked and therefore have relatively weak SV.

3.4. Comparison with Réunion and Hawai'i

Finally we make a comparison between these dynamo models and data from the volcanic islands of Hawai'i and Réunion using the recent comprehensive study of Love and Constable (2003). These two sites were chosen because they have almost exactly opposite latitudes and could therefore be used to detect departures from equatorial symmetry, assuming no persistent variation with longitude.

Tables 2 and 3 display time-averaged directional data for Hawai'i and Réunion Island for the three values of ϵ and the observed means from Love and Constable (2003). The Hawai'iian table shows a clear decrease (increase) in time-averaged inclination (declination) with increasing ϵ . Decreasing inclination corresponds to the emergence of a large negative inclination anomaly in the region (see Fig. 3). Growth of D is probably because of the increased amplitude of non-zonal harmonics as ϵ increases. The results for $\epsilon = 0.9$ are the closest to the observations; data for $\epsilon = 0.3$ and 0.6 do not provide a good fit.

The picture changes for Réunion, however, with no systematic change in I or D as ϵ changes. There is a large shift between $\epsilon = 0.6$ and 0.9 , with D decreasing by 5.1° and I increasing by 3.9° . The shift in I occurs because of the large positive inclination anomaly in the $\epsilon = 0.9$ solution. Again, a large value of D for $\epsilon = 0.9$ is due to the greater amplitude of non-zonal terms. The $\epsilon = 0.6$ solution gives the closest match to the observed Réunion data.

Love and Constable (2003) draw attention to the large difference (9°) in inclination between the two sites. For our dynamo models the difference in mean inclination is 3.56° for $\epsilon = 0.6$ and 2.96° for $\epsilon = 0.9$. The inclination plot in Fig. 3 shows that the difference in inclination for the model is caused by the large positive anomaly centered on southern Africa and the negative anomaly in the Pacific, but Réunion lies close to the edge of the big positive anomaly and a small displacement in longitude, as is achieved by changing some of the other dynamo parameters, would make a big difference to the predicted inclination. We conclude that differences between the sites are more likely to result from longitudinal variations in I than any equatorial asymmetry.

There are also clear differences in D between the two sites. Values of σ_D in Table 2 do not differ significantly between Hawai'i and Réunion, whereas Love and Constable (2003) find the histogram for D in Hawai'i to be significantly narrower than a Gaussian. This suggests weak SV in the Pacific data; the dynamo models do not show weak SV.

Fig. 7 shows histograms of I and D for Hawai'i and Réunion with the best-fitting Gaussian probability density functions. The inclination and declination data are well fit by a Gaussian while the intensity data shows a worse fit.

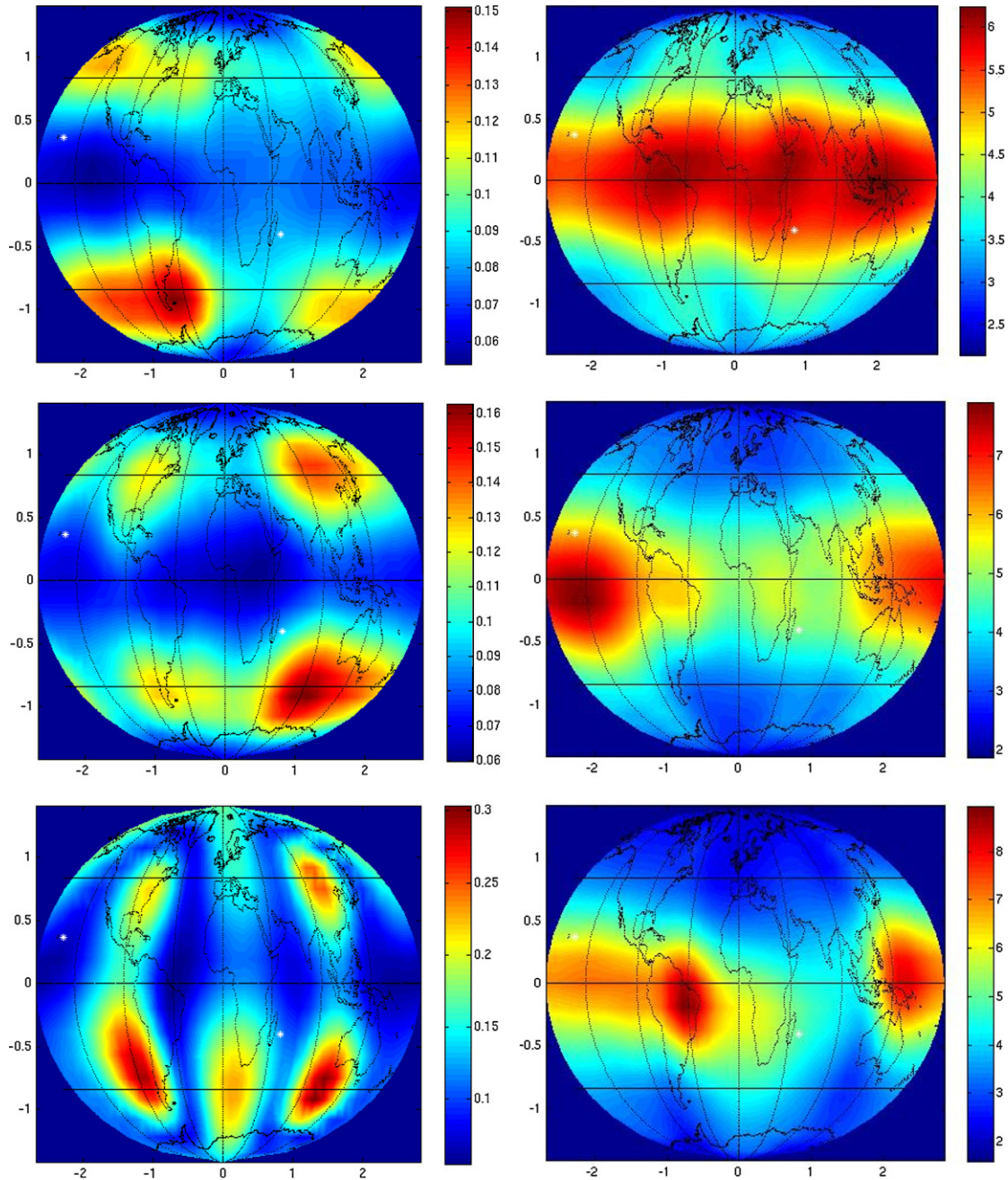


Fig. 5. σ_F (left column) and σ_1 (right column) for $\epsilon = 0.3$ (top row), $\epsilon = 0.6$ (middle row) and $\epsilon = 0.9$ (bottom row). σ_D has not been plotted as the plots are dominated by the increase towards the poles. Similarities between σ_F and ΔF suggest that SV takes the form of pulsations of the main flux lobes rather than drift. Confinement of large σ_1 to equatorial regions demonstrates the large SV at low latitudes.

4. Summary, discussion and conclusions

We have compared dynamo solutions with paleomagnetic data. We only vary the parameter ϵ that determines the strength of the boundary heterogeneity and are therefore only testing the effect of the boundary conditions. We are also testing the hypothesis that lower mantle shear-wave anomalies are caused by temperature rather than composition. We have argued that the dynamo-generated fields can be separated into two parts, a locked part that is relatively stationary and a time-varying part with persistent centres of activity that give it a non-zero time average: both contribute to the time average. Increasing the boundary heterogeneity leads to stronger locked fields relative to time-varying fields. The

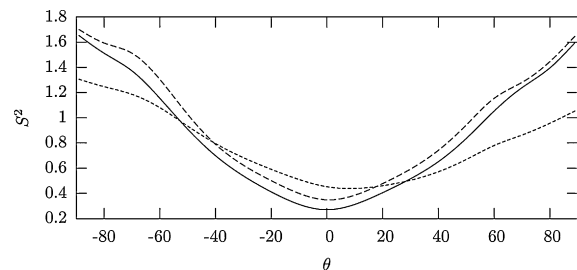


Fig. 6. VGP scatter function, defined by Eq. (2), as a function of latitude for $\epsilon = 0.3$ (solid line), $\epsilon = 0.6$ (dashed line) and $\epsilon = 0.9$ (short-dashed line). Note the clear equatorial symmetry of S^2 and monotonic increase towards the poles.

Table 2
Time-averaged directional data at Hawai'i for each of the three models

Model	I (°)	D (°)	σ_I	σ_D
$\epsilon = 0.3$	34.18	0.44	4.44	3.81
$\epsilon = 0.6$	33.27	0.58	6.30	4.56
$\epsilon = 0.9$	29.99	3.61	5.92	4.64
Love and Constable (2003)	30.49	0.11	–	–

Data from Love and Constable (2003) is also included. $\epsilon = 0.9$ provides the closest fit to the observations.

Table 3
Time-averaged directional data at Réunion for each of the three models

Model	I (°)	D (°)	σ_I	σ_D
$\epsilon = 0.3$	–35.47	0.04	4.93	3.95
$\epsilon = 0.6$	–36.83	–1.82	4.79	4.26
$\epsilon = 0.9$	–32.93	–6.93	4.91	4.41
Love and Constable (2003)	–39.99	–0.69	–	–

Data from Love and Constable (2003) is also included. $\epsilon = 0.6$ provides the closest match to the data.

time averages are dependent on ϵ to a surprising degree, which we attribute to variations in the proportions of locked and time-varying contributions to the field.

The averaging time required to produce a rough time average, one where further changes are below the threshold set by paleomagnetic data, can be fairly short, 150–500 kyr or 1.5–5 magnetic diffusion times; this averaging time decreases with ϵ because the boundary inhomogeneities reduce the time-varying part of the field. However, the averaging time to produce an accurate time average can be much longer, over 1 Myr or 10 diffusion times, because the boundary anomalies can cause the field to “hang up” for significant lengths of time before switching into a new interval of rapid change. It cannot therefore be argued that averaging times will always decrease with ϵ , although they do here. Paleomagnetic data can be used to estimate the time to achieve a rough time average, but inaccuracies in the data mean that they cannot be used to determine the time for an accurate time average and therefore probably cannot detect boundary control of the field.

Axisymmetric time averages are dominated by peaks and troughs in inclination anomaly at high and low latitudes, the former

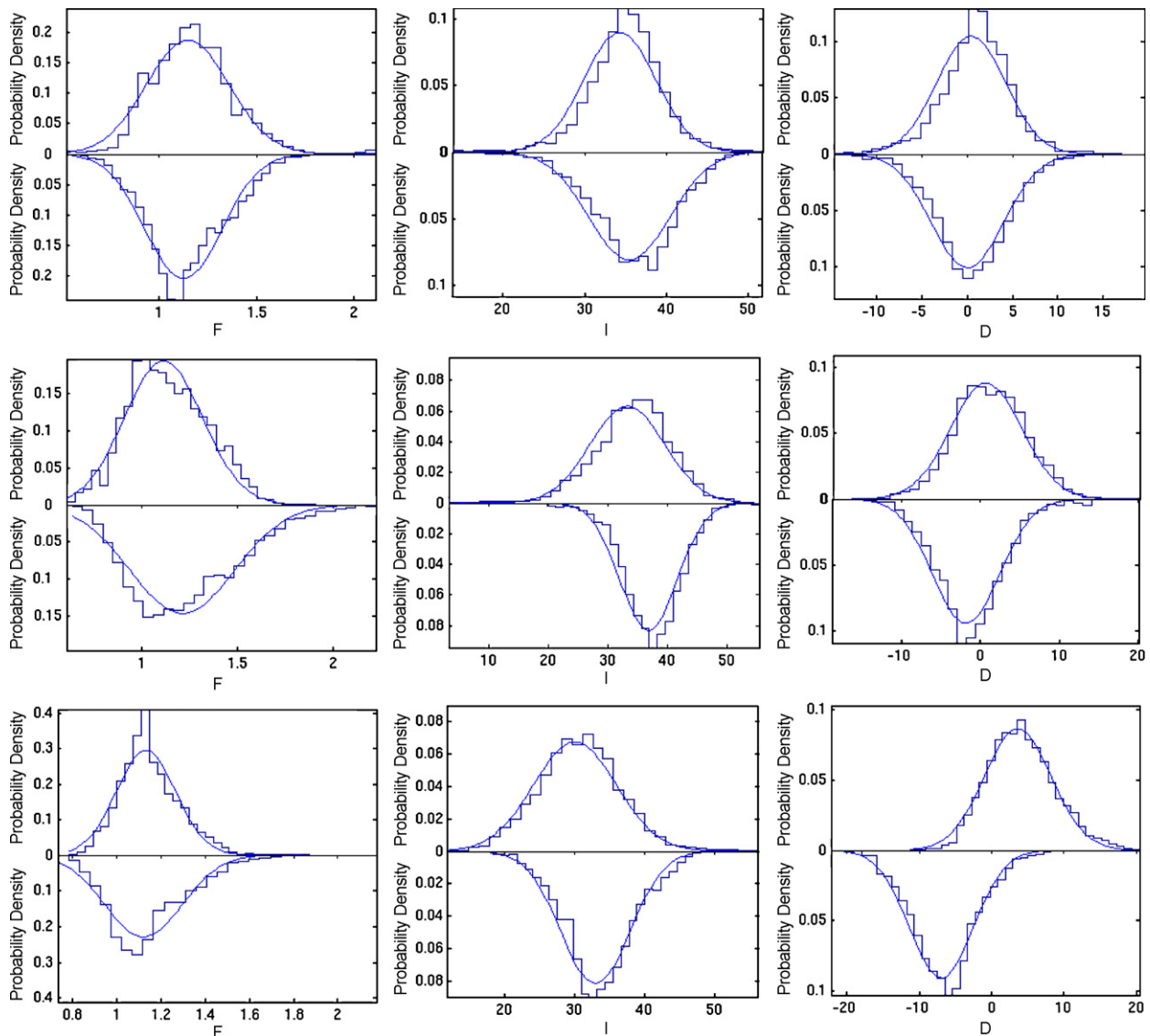


Fig. 7. Histograms of F (left), I (middle) and D (right) for the three cases $\epsilon = 0.3$ (top row), $\epsilon = 0.6$ (middle row) and $\epsilon = 0.9$ (bottom row). Hawai'i data are shown positive top and Réunion data negative bottom in each figure. The sign of I for Réunion results has been changed to facilitate comparison with the Hawai'i data. The best-fitting Gaussian probability density function is indicated by a solid line. I and D are well-fit by Gaussian distributions while F is not. Differences in mean declination increase with ϵ .

associated with the locked field and the latter with the time-averaged time-varying field. Relative geomagnetic coefficients G_2^0 and G_3^0 are smaller than estimates from paleomagnetic data and have mainly different signs; G_3^0 dominates, probably because the dynamo fields are strongly symmetrical about the equator. Axisymmetric intensities are undetectably different from those of a dipole field except within 20° of the poles, resulting from lack of flux within the tangent cylinder.

The full time average is dominated by non-axisymmetric geomagnetic coefficients, the largest being G_3^2 , G_2^1 and G_1^1 in the locked $\epsilon = 0.9$ solution. The inclination anomaly for the locked solution shows dramatic $\pm 8^\circ$ variation in longitude; it gives a strong negative anomaly in the Pacific in agreement with observation. The same model predicts a difference in inclination between Hawai'i and Réunion that agrees with observation but no difference in declination. Lower values of ϵ do not give good agreement with observation. Secular variation in the models is high in equatorial latitudes, in agreement with the observational model of Korte and Constable (2005). Secular variation is not low in the Pacific hemisphere.

The closest study to this one is that of Olson and Christensen (2002), who employed a tomographic boundary condition for some of their solutions. The principal difference is their choice of Roberts number, $q = 1$ or 2 compared with our 10, and a correspondingly higher Rayleigh number to compensate for the higher diffusivity and provide dynamo action. The magnetic Reynolds numbers of both studies are comparable at $R_m = 500$. Their choice of Ekman numbers brackets ours, and they truncate their tomographic boundary condition at spherical harmonic degree 4 whereas we use the full set to degree 12. Their high Ra leads to more rapidly time-varying solutions. Their time-averaged axisymmetric solutions are dominated by a large and positive G_3^0 and almost zero G_2^0 . This agrees with our $\epsilon = 0.3$ and 0.6 solution but there is a striking change with the $\epsilon = 0.9$ solution, where G_3^0 changes sign (Table 1). This suggests the Olson and Christensen (2002) time average is dominated by the time-varying part of their solution, as with our $\epsilon = 0.3$ and 0.6, rather than the locked part, as with our $\epsilon = 0.9$, as expected from the high values of Ra employed.

Olson and Christensen (2002) also comment on an azimuthal phase shift between the time-averaged field and the boundary heating pattern, and attribute this to the large Ekman number. Our solutions do not show such a shift, and give excellent agreement with the longitudes of the main lobes of the modern field, so we suggest the shift is caused by averaging of secular variation events in their model rather than a shift in the locked field. Our solutions do not show spiralling of the convection rolls; in fact changing the parameters to produce spiralling tends to destroy the dynamo action (B. Sreenivasan, personal communication).

The most striking result of this paper is the strong longitudinal variation in inclination anomaly (Fig. 3), which is larger than the latitudinal variation. The Island of Réunion lies near the eastern edge of the African positive anomaly; a slight eastward movement of the anomaly would change the predicted inclination significantly, bringing it into line with the observed average of Love and Constable (2003). Clearly Hawai'i and Réunion are a poor choice of sites to detect north–south asymmetry, since sites that were on the same longitude would have detected, according to this map, asymmetry for Hawai'i's longitude but no asymmetry for Réunion's longitude. Symmetry of the VGP scatter curves gives us confidence in the common paleomagnetic practise of averaging both hemispheres, but the shape of the curve seems a poor way to estimated PSV. First, axisymmetric averaging removes any strong longitudinal variation, and secondly it is biased towards high values at the poles simply by the mathematical transformation.

We conclude that paleomagnetic data adds some additional support for a dynamo controlled by boundary heat flux anomalies, and that those heat flux anomalies are adequately predicted by lower mantle shear-wave velocities. The locked part of the fields agree remarkably well with the more stable part of the modern geomagnetic field, the four main lobes that comprise the dipole, and some aspects of the time-averaged paleomagnetic field. The locked field fits the paleomagnetic data better than the time-averaged time-varying part, suggesting that we should study dynamos with fields that are substantially locked to the boundary rather than time averages of chaotic solutions. Furthermore, the match of the locked solution with the modern field suggests to us that the geomagnetic field spends a great deal of its time in this four-lobe configuration: it is not a coincidence that we live at a time when the field resembles its long-term average. This presents a great challenge to the dynamo theory because any changes to the parameters that would make the model more “geophysically realistic”, such as lower E , higher Ra , or lower q , are likely to destroy the locked solution. Lastly, our magnetic fields are dominated by non-axisymmetric terms, so an axisymmetric average will lead to biased results if the geographical data coverage is not longitudinally uniform.

Acknowledgements

This work was supported by NERC Consortium Grant *Deep Earth Systems O/2001/00668*. C. Davies is supported by a NERC E-science research studentship. We thank an anonymous reviewer for their comments.

References

- Aubert, J., Amit, H., Hulot, G., 2007. Detecting thermal boundary control in surface flows from numerical dynamos. *Phys. Earth Planet. Int.* 160, 143–156.
- Bloxham, J., 2000. The effect of thermal core–mantle interactions on the palaeomagnetic secular variation. *Phil. Trans. R. Soc. Lond. A* 358, 1171–1179.
- Bloxham, J., 2002. Time-independent and time-dependent behaviour of high-latitude flux bundles at the core–mantle boundary. *Geophys. Res. Lett.* 29, 1–4.
- Bloxham, J., Gubbins, D., 1985. The secular variation of the Earth's magnetic field. *Nature* 317, 777–781.
- Carlut, J., Courtillot, V., Hulot, G., 1999. Over how much time should the geomagnetic field be averaged to obtain the mean paleomagnetic field? *Terra Nova* 11, 239–243.
- Christensen, U., Olson, P., 2003. Secular variation in numerical geodynamo models with lateral variations of boundary heat flow. *Phys. Earth Planet. Int.* 138, 39–54.
- Constable, C., Johnson, C., Lund, P., 2000. Global geomagnetic field models for the past 3000 years: transient or permanent flux lobes? *Phil. Trans. R. Soc. Lond. A* 358, 991–1008.
- Doell, R., Cox, A., 1972. The Pacific secular variation anomaly and the question of lateral uniformity in the lower mantle. In: Robertson, E. (Ed.), *The Nature of the Solid Earth*. McGraw-Hill, New York, NY, pp. 245–284.
- Elmaleh, A., Valet, J., Herrero-Bervera, E., 2001. A map of the Pacific geomagnetic anomaly during the Brunhes chron. *Earth Planet. Sci. Lett.* 193, 315–332.
- Glatzmaier, G., Coe, R., Hongre, L., Roberts, P., 1999. The role of the earth's mantle in controlling the frequency of geomagnetic reversals. *Nature* 401, 885–890.
- Gubbins, D., 1998. Interpreting the paleomagnetic field. In: *The Core–Mantle Boundary Region*, vol. 28. American Geophysical Union, pp. 167–182.
- Gubbins, D., Kelly, P., 1995. On the analysis of paleomagnetic secular variation. *J. Geophys. Res.* 100, 14955–14964.
- Gubbins, D., Willis, A., Sreenivasan, B., 2007. Correlation of Earth's magnetic field with lower mantle thermal and seismic structure. *Phys. Earth Planet. Int.* 162, 256–260.
- Herrero-Bervera, E., Valet, J., 2003. Persistent anomalous inclinations recorded in the Koolau volcanic series on the island of Oahu (Hawaii, USA) between 1.8 and 2.6 Ma. *Earth Planet. Sci. Lett.* 212.
- Jackson, A., Finlay, C., 2007. Geomagnetic secular variation and its applications to the core. In: Schubert, G. (Ed.), *Treatise on Geophysics*. Elsevier.
- Jackson, A., Jonker, A., Walker, M., 2000. Four centuries of geomagnetic secular variation from historical records. *Phil. Trans. R. Soc. Lond. A* 358, 957–990.
- Johnson, C., Constable, C., 1995. The time-averaged field as recorded by lava flows over the past 5 Myr. *Geophys. J. Int.* 122, 489.
- Johnson, C., Constable, C., 1998. Persistently anomalous Pacific geomagnetic fields. *Geophys. Res. Lett.* 25, 1011–1014.
- Kelly, P., Gubbins, D., 1997. The geomagnetic field over the past 5 million years. *Geophys. J. Int.* 128, 315–330.

- Korte, M., Constable, C., 2005. Continuous geomagnetic field models for the past 7 millennia: 2.CALS7K. *Geochem. Geophys. Geosys.* 6, 1–18.
- Kutzner, C., Christensen, U., 2004. Simulated geomagnetic reversals and preferred geomagnetic pole paths. *Geophys. J. Int.* 157, 1105–1118.
- Laj, C., Mazaud, A., Weeks, R., Fuller, M., Herrero-Bervera, E., 1991. Geomagnetic reversal paths. *Nature* 351, 447.
- Love, J., 1998. Paleomagnetic volcanic data and geometric regularity of reversals and excursions. *J. Geophys. Res.* 103, 12435–12452.
- Love, J., Constable, C., 2003. Gaussian statistics for palaeomagnetic vectors. *Geophys. J. Int.* 152, 515–565.
- Masters, G., Johnson, S., Laske, G., Bolton, H., 1996. A shear-velocity model of the mantle. *Phil. Trans. R. Soc. Lond. A* 354, 1385–1411.
- McFadden, P., Merrill, R., McEhinney, M., 1988. Dipole/quadrupole family modelling of paleosecular variation. *J. Geophys. Res.* 93, 11583–11588.
- McFadden, P., Merrill, R., McEhinney, M., Lee, S., 1991. Reversals of the Earth's magnetic field and temporal variations of the dynamo families. *J. Geophys. Res.* 96, 3923–3933.
- Merrill, R., McFadden, P., 2003. The geomagnetic axial dipole field assumption. *Phys. Earth Planet. Int.* 139, 171–185.
- Merrill, R.T., McElhinny, M.W., McFadden, P.L., 1996. *The Magnetic Field of the Earth—Paleomagnetism, the Core, and the Deep Mantle*: vol. 63 of International Geophysics Series. Academic Press, San Diego.
- Olson, P., Christensen, U., 2002. The time-averaged magnetic field in numerical dynamos with non-uniform boundary heat flow. *Geophys. J. Int.* 151, 809–823.
- Sarson, G., Jones, C., Longbottom, A., 1997. The influence of boundary region heterogeneities on the geodynamo. *Phys. Earth Planet. Int.* 101, 13–32.
- Sreenivasan, B., Gubbins, D., 2008. Dynamos with weakly convecting outer layers: implications for core-mantle boundary interaction. *Geophys. Astrophys. Fluid Dynam.* 102, 395–407.
- Willis, A., Sreenivasan, B., Gubbins, D., 2007. Thermal core-mantle interaction: exploring regimes for 'locked' dynamo action. *Phys. Earth Planet. Int.* 165, 83–92.
- Zhang, K., Gubbins, D., 1993. Convection in a rotating spherical fluid shell with an inhomogeneous temperature boundary condition at infinite Prandtl number. *J. Fluid Mech.* 250, 209–232.